SECURITY INFORMATION

[redacted]

Copy
RM L53J12a

TECH LIBRARY KAFB, NM
0144301

NACA RM L53J12a

7494

[redacted]

NACA

RESEARCH MEMORANDUM

LONGITUDINAL STABILITY AND TRIM OF TWO ROCKET-PROPELLED AIRPLANE MODELS HAVING 45° SWEPTBACK WINGS AND TAILS WITH THE HORIZONTAL TAIL MOUNTED IN TWO POSITIONS

By James H. Parks and Alan B. Kehlet

Langley Aeronautical Laboratory
Langley Field, Va.

Unclassified
Nasa Tech Pub Announcement #108
By 2 Nov 56
NK
GRADE OF OFFICER MAKING CHANGE)
4 Apr 61 CLASSIFIED DOCUMENT
[redacted] person is prohibited by law.

NATIONAL ADVISORY COMMITTEE FOR AERONAUTICS

WASHINGTON

December 9, 1953

[redacted]

[redacted]

 [redacted]

TECH LIBRARY KAFB, NM

0144301

NATIONAL ADVISORY COMMITTEE FOR AERONAUTICS

RESEARCH MEMORANDUM

LONGITUDINAL STABILITY AND TRIM OF TWO ROCKET-PROPELLED AIRPLANE MODELS HAVING 45° SWEPTBACK WINGS AND TAILS WITH THE HORIZONTAL TAIL MOUNTED IN TWO POSITIONS

By James H. Parks and Alan B. Kehlet

SUMMARY

Results are presented at Mach numbers from 0.60 to 1.40 of a free-flight investigation of the longitudinal stability, trim, and horizontal-tail vibration characteristics of two rocket-propelled airplane models at low lift coefficients. The configurations had the same wing—body—vertical-tail combination with one model having the horizontal tail mounted on the fuselage center line and the other having the horizontal tail mounted atop the vertical tail. All airfoil surfaces were swept back 45° and the wings and horizontal tail had aspect ratio of 4, taper ratio of 0.6, and thickness ratio of 6 percent. The horizontal tails were fixed at 2° incidence, trailing edge down, on both models.

The lift-curve slopes were approximately equal for both models at Mach numbers where they could be compared. Both configurations were statically stable in the longitudinal mode and exhibited stable longitudinal damping characteristics over the speed range investigated. Longitudinal trim changes, in a nose-up direction, occurred in both flight tests at transonic speeds.

The horizontal tails on both models encountered objectionable vibrations at frequencies near the respective first bending mode of the horizontal tails throughout the Mach number range investigated.

INTRODUCTION

As previously reported in reference 1, a general research program is being conducted by the National Advisory Committee for Aeronautics to determine, by means of rocket-propelled models in free flight, the effects of various empennage designs on the longitudinal aerodynamic characteristics of complete airplane configurations at transonic speeds.

[redacted]

[redacted]

[redacted]

Presented herein are the results of two tests employing models of a basic wing—fuselage—vertical-tail configuration with horizontal tails of the same geometry but at different tail heights. The horizontal tails of both models were fixed at 2° incidence, trailing edge down.

The models contained vertically-thrusting pulse rockets arranged to produce disturbances from the trim condition in the longitudinal mode of motion. The flight tests were conducted at the Pilotless Aircraft Research Station at Wallops Island, Va.

In the interest of expediting publication of the data, the results of the present two tests in the series are presented without a complete analysis but with some qualitative discussion.

SYMBOLS

b	wing span, ft
c	chord, ft
$\bar{c}$	mean aerodynamic chord, $\dfrac{\int_0^{b/2} c^2 dy}{\int_0^{b/2} c\, dy}$, ft
g	gravitational acceleration, ft/sec^2
q	dynamic pressure, lb/sq ft
y	spanwise wing station, ft
I_y	moment of inertia about y-axis, slug-ft^2
M	Mach number
R	Reynolds number, based on $\bar{c}$
S	wing area, sq ft
V	velocity, ft/sec
W	weight of model, lb
a_n/g	normal accelerometer reading, positive up
α	angle of attack, deg[redacted]

[redacted]

[redacted]

θ angle of pitch, radians

C_N normal-force coefficient, $\frac{Wa_n}{Sqg}$

C_L lift coefficient, $C_N \cos \alpha$

C_m pitching-moment coefficient about the center of gravity, $\frac{\text{Pitching moment}}{qS\bar{c}}$

Subscripts:

$\dot{\alpha} = \frac{1}{57.3} \frac{\bar{c}}{2V} \frac{da}{dt}$

$q = \frac{\bar{c}}{2V} \frac{d\theta}{dt}$

Symbols used as subscripts indicate the derivative of the quantity with respect to the quantity, for example $C_{L_\alpha} = \frac{dC_L}{d\alpha}$.

MODELS AND INSTRUMENTATION

Three-view drawings of the models are shown in figure 1. The model having the horizontal tail in the low position is designated model A and the high-tail configuration, model B. Photographs of the models are shown in figure 2. Details of construction are given in reference 1. Briefly, however, the models were constructed primarily of laminated mahogany with metal plates incorporated in the wing and horizontal tail for additional stiffness and rigidity.

The wings and horizontal tails on both models had an aspect ratio of 4, taper ratio of 0.60, and NACA 65A006 airfoil sections in the streamwise direction with the quarter-chord line swept back 45°. The vertical tail had an aspect ratio of 1.5, taper ratio of 0.50, and NACA 65A008 airfoil section in the streamwise direction with the quarter-chord line swept back 45°. The wing had zero incidence while the horizontal tails in both cases were fixed at 2°, trailing edge down. Both horizontal tails had the same total area.

The fuselage was a parabolic body of revolution of fineness ratio 8.91 with maximum thickness at 40 percent of the length. Fuselage ordinates are tabulated in reference 1.

The models were boosted to maximum velocity by ABL Deacon rocket motors. A model-booster combination (low-tail model) is shown on the launching platform at the launching angle of 60° elevation in figure 3. The vertically-thrusting pulse-rocket installation used to produce longitudinal oscillations is described in reference 1. Each pulse rocket had a total impulse of approximately 8 pound-seconds and a burning time of approximately 0.08 second.

The models were equipped with NACA four-channel telemeters which transmitted continuous records of normal acceleration, angle of attack, total pressure, and a measure of the frequency and amplitude of the horizontal-tail vibrations. A photograph of the tail vibration pickup in the high tail model is shown in figure 4.

The flight paths were determined from tracking radar data and atmospheric conditions at altitude were obtained from radiosondes released immediately after model launchings.

A detailed discussion of the data analysis technique and accuracy of this type of investigation is found in references 1 and 2. For the particular instrumentation used, the absolute accuracy in C_L is ± 0.01 at $M = 1.20$ and ± 0.02 at $M = 0.80$. The angle of attack is believed correct within $\pm 0.20^{\circ}$ and the Mach number is estimated to be within 0.02 at $M = 1.00$. It might be noted that the lift coefficient is defined as a function of normal force only (see section entitled "Symbols"); the error introduced by omission of the contribution of the chord force is believed negligible.

Not much experience has been acquired with the vibration pickup; however, for the present tests, it is estimated that the frequencies are correct within 5 cycles per second. The pickup is designed as a frequency indicator and amplitudes indicated by the instrument may be in error by as much as ± 25 percent. Some amplitude data are included herein but are presented as a qualitative indication only.

RESULTS AND DISCUSSION

The dynamic pressures and Reynolds numbers for these tests are shown in figures 5 and 6, respectively. It should be emphasized that, as shown in figure 7, all data are in the low lift range.

Although the two models are quite similar, the differences in horizontal-tail locations introduce several factors which must be considered in comparing their aerodynamic characteristics. The following are considered of primary importance: the loss of lifting ability due to the greater flexibility of the high tail resulting from its greater

exposed span, the increased tail length resulting from moving the tail off the fuselage center line to the top of the vertical tail, the differences in flow conditions in the regions of the respective tail positions arising both from the wing wake and downwash effects and the effects of the fuselage on the flow. It should be noted that the center-of-gravity positions for models A and B were 9 and 4 percent $\bar{c}$, respectively.

Lift.- The lift curves obtained are plotted in figure 7. Although some scatter exists, all data appear linear. The lift-curve slopes represented by the faired lines in figure 7 are shown as a function of Mach number in figure 8. Since the major part of the lift is generated by the wing, both models exhibit generally the same lifting capabilities.

No lift-curve slope is presented for the data shown for model B in figure 7(b) at $M = 1.28$ because of the very limited amplitude of the oscillation.

The data of references 1 and 3 were used to estimate the losses in lift-curve slope for model A arising from flexibility. This correction, shown in figure 9, is not precise but does indicate the order of magnitude of these losses. The order of magnitude shown is also applicable to model B.

Static longitudinal stability.- The periods of the short-period oscillation were used to determine the static stability parameter C_{m_α}. These data are shown in figure 10 as a function of Mach number. Although no quantitative assessment is made, it should be noted that particularly the high tail was probably affected by altered local flow conditions arising from strong base shocks which were indicated to exist on a geometrically similar afterbody by the results of reference 4.

The degree of longitudinal stability, as indicated by the aerodynamic-center locations, is shown in figure 11. The C_{L_α} data for model A were used to compute this parameter for model B at Mach numbers greater than 1.12 but the error introduced is believed small. Also it is pointed out that the forward movement of the aerodynamic center indicated for model B at these Mach numbers may be to some extent affected by the relatively low amplitudes of the basic data at $M = 1.28$ (fig. 7(b)) if the pitching-moment variation with angle of attack is nonlinear near $\alpha = 2^\circ$.

It might be well to emphasize that these data are for the low lift condition only. At higher angles of attack, the stability may be considerably different. This effect is discussed in detail in reference 5.

Dynamic longitudinal stability.- The times required for the short-period oscillation to damp to one-half amplitude were used to calculate the dynamic longitudinal stability characteristics. Damping-moment

factors corresponding to these time increments are shown in figure 12. The damping moment is stable over the entire Mach number range tested for both models. It might be noted that although the damping moment for model A decreases to quite low values near $M = 0.95$, the lift contribution to the total damping is near maximum values at these speeds (fig. 8). The trends indicated are in general agreement with the results of reference 6.

Longitudinal trim.- The trim lift coefficients for both configurations through the Mach number range are shown in figure 13(a). The shape of the trim curves agrees favorably with previous rocket model tests in configurations of this type. The increment of nose-up pitching moment arising from the drag of the high horizontal tail is believed to be a relatively small contributing factor to the larger trim change exhibited by model B.

The angle of attack corresponding to these trim lift conditions is shown in figure 13(b). No unusual variations are noted. Although the variation in angle of attack for each model is considered quite reliable, the absolute accuracy of the angle-of-attack data, discussed in the section "Model and Instrumentation" must be considered when comparing the levels of these curves.

Tail vibrations.- The horizontal tails of both models vibrated throughout the flight although it was estimated that neither tail should encounter classical flutter at the Mach numbers of the tests, and it is generally recognized that isolated airfoils having the geometry of the horizontal tails should not buffet. The predominant frequencies of these vibrations are presented in figure 14 as a function of Mach number. Also shown in the figure are the basic natural frequencies of the wings and tails as determined by vibration tests prior to flight testing.

Both tails generally showed similar vibration frequency variations; near $M = 0.70$ both exhibit frequencies very near the respective horizontal-tail first bending frequencies and near $M = 1.30$ both vibrated at approximately 130 percent of these values with the most rapid changes occurring near $M = 0.85$.

The absence of similar indications in the normal accelerations recorded at the model center-of-gravity locations is evidence that these vibrations are largely localized in the empennage.

It should be noted that the vertical tail may be a contributing factor to the empennage vibrations because of its greater thickness ratio (8 percent); however, no data are readily available for comparative purposes.

Although the vibration pickup is not designed as a reliable source of vibration amplitudes, figure 15 is included to show the nature of the

vibrations at a representative Mach number and figure 16 is included to indicate the order of magnitude of the vibrations as a function of flight time and Mach number. When comparing these amplitude data, it should be noted that vibration pickups were located near the tips of the horizontal tails and thus the pickup in the high tail was considerably further from the effective structural root than was the pickup in the low tail. Assuming freedom in bending only, it is estimated that this factor should, for a given input, cause the amplitude response indicated for the high tail to be 2.5 times a corresponding value for the low tail.

Beyond the fact that these vibrations are very objectionable and might reach destructive amplitudes at higher lift coefficients, true assessment is virtually impossible from these data alone.

CONCLUDING REMARKS

Two rocket-propelled models having 45° sweptback wings and tails, one having the horizontal tail on the fuselage center line and the other having the horizontal tail mounted atop the vertical tail, were flight-tested at low lift coefficients. At the center-of-gravity positions employed, both models exhibited generally the same lifting capabilities and were statically and dynamically stable in the longitudinal mode at low lift over the entire Mach number range. Both models underwent longitudinal trim changes in the nose-up direction at transonic speeds. Considerable differences in the stability and trim characteristics for the two models are shown but no quantitative analysis is presented. The horizontal tails of both models experienced objectionable vibrations with frequencies near the respective horizontal-tail first bending modes.

Langley Aeronautical Laboratory,
National Advisory Committee for Aeronautics,
Langley Field, Va., September 29, 1953.

[redacted]

REFERENCES

1. Parks, James H., and Kehlet, Alan B.: Longitudinal Stability, Trim, and Drag Characteristics of a Rocket-Propelled Model of an Airplane Configuration Having a 45° Sweptback Wing and an Unswept Horizontal Tail. NACA RM L52F05, 1952.

2. Gillis, Clarence L., Peck, Robert F., and Vitale, A. James: Preliminary Results From a Free-Flight Investigation at Transonic and Supersonic Speeds of the Longitudinal Stability and Control Characteristics of an Airplane Configuration With a Thin Straight Wing of Aspect Ratio 3. NACA RM L9K25a, 1950.

3. Vitale, A. James: Effects of Wing Elasticity on the Aerodynamic Characteristics of an Airplane Configuration Having 45° Sweptback Wings As Obtained From Free-Flight Rocket-Model Tests at Transonic Speeds. NACA RM L52L30, 1953.

4. Katz, Ellis R., and Stoney, William E., Jr.: Base Pressures Measured on Several Parabolic-Arc Bodies of Revolution in Free Flight at Mach Numbers From 0.8 to 1.4 and at Large Reynolds Numbers. NACA RM L51F29, 1951.

5. Mitchell, Jesse L.: The Static and Dynamic Longitudinal Stability Characteristics of Some Supersonic Aircraft Configurations. NACA RM L52A10a, 1952.

6. Gillis, Clarence L., and Chapman, Rowe, Jr.: Summary of Pitch-Damping Derivatives of Complete Airplane and Missile Configurations As Measured in Flight at Transonic and Supersonic Speeds. NACA RM L52K20, 1953.

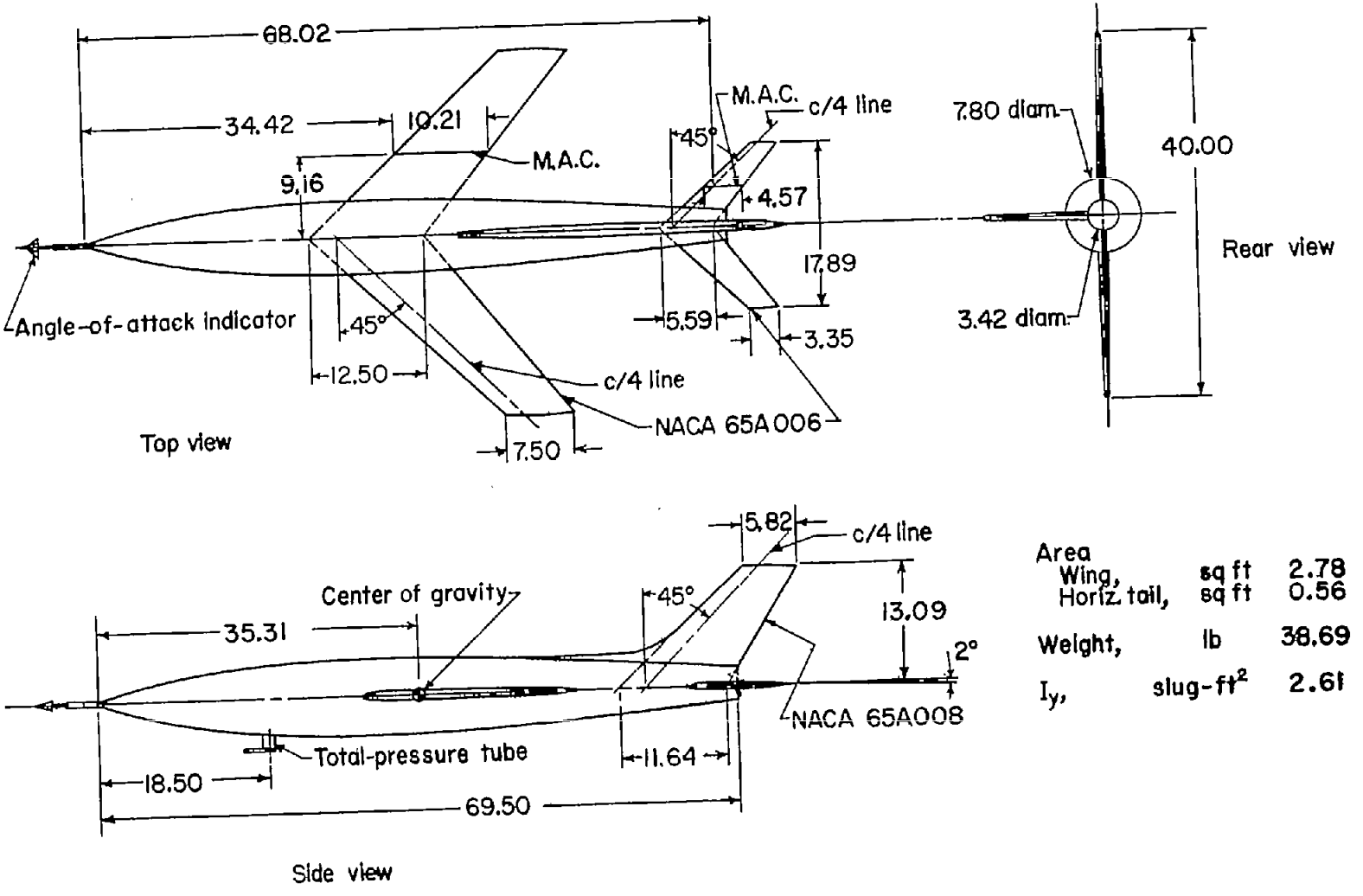

Area		
Wing,	sq ft	2.78
Horiz. tail,	sq ft	0.56
Weight,	lb	38.69
I_y,	slug-ft^2	2.61

(a) Model A.

Figure 1.- General arrangement of model A and model B. All dimensions are in inches.

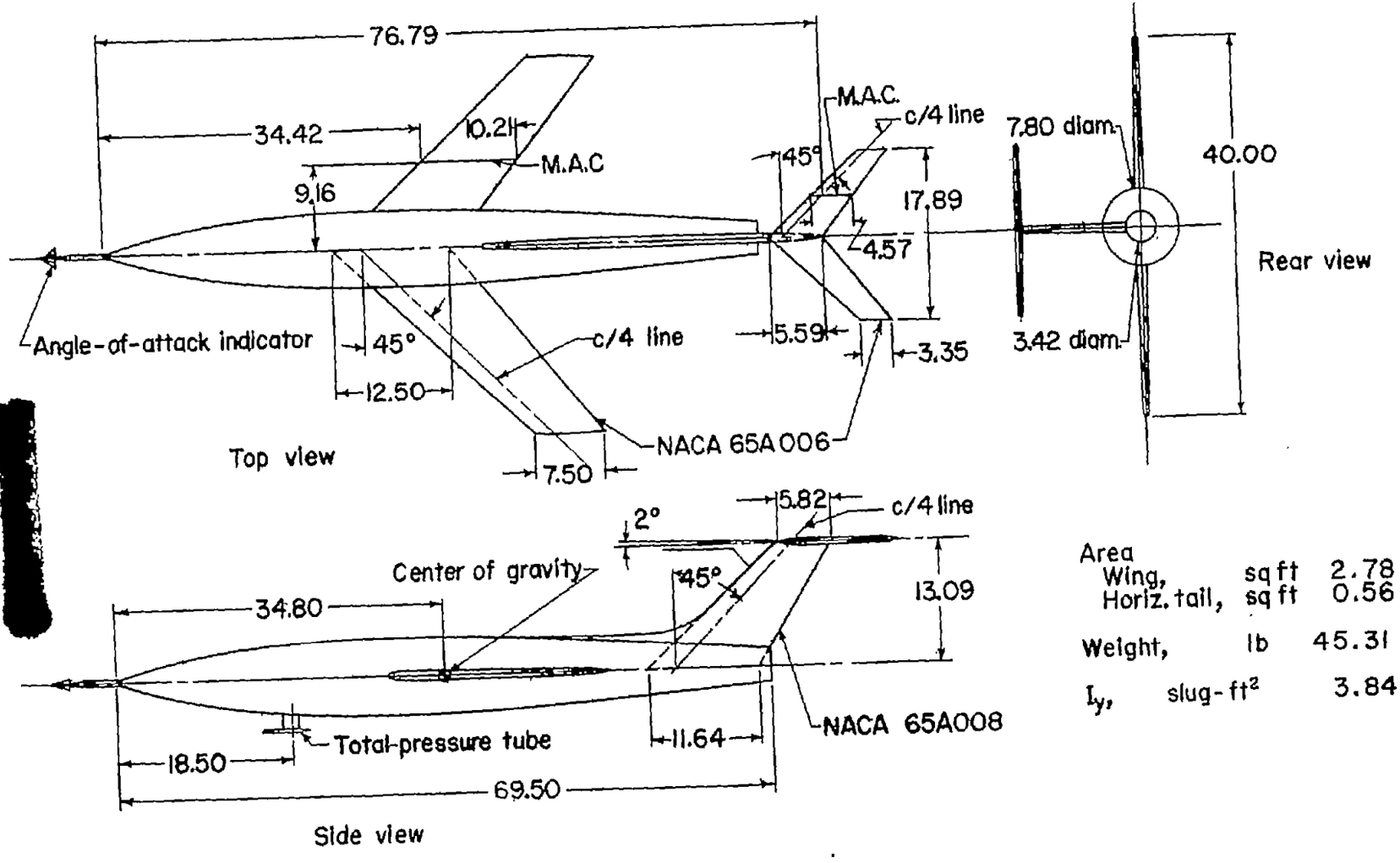

Area		
Wing,	sq ft	2.78
Horiz. tail,	sq ft	0.56
Weight,	lb	45.31
I_y,	slug-ft^2	3.84

(b) Model B.

Figure 1.- Concluded.

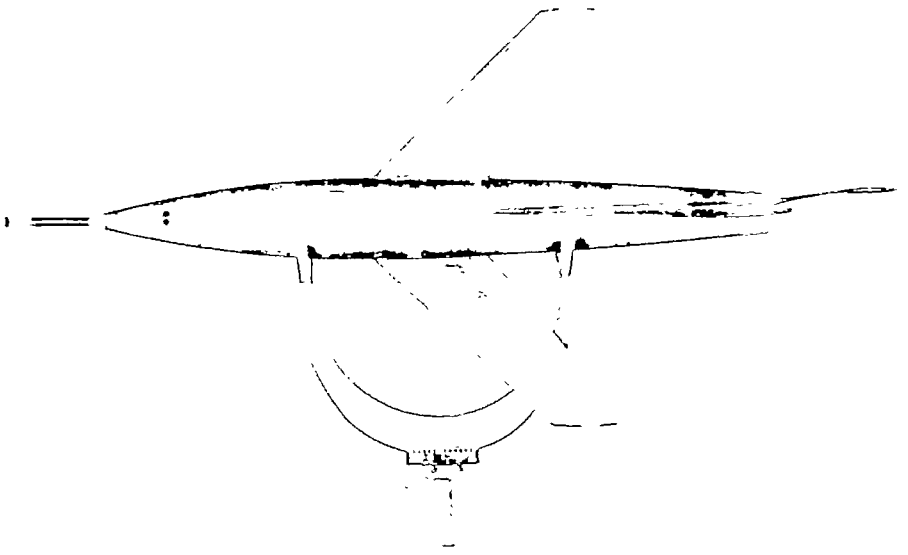

Top view L-78184.1

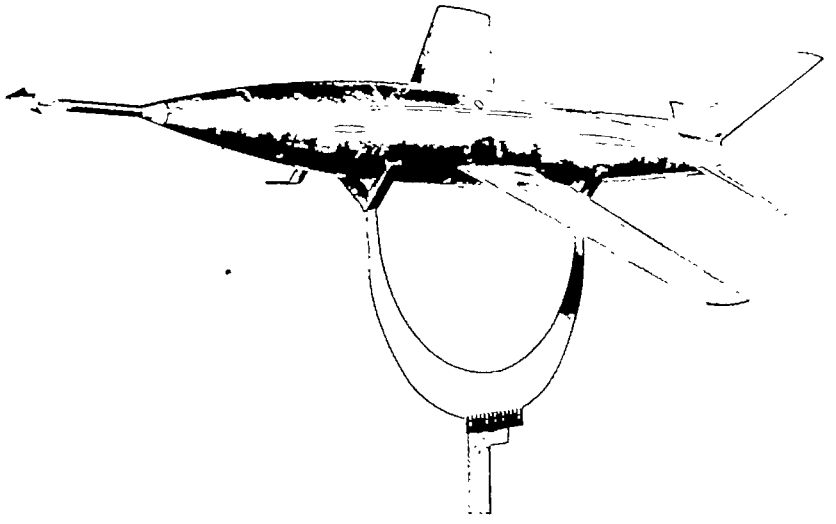

Three-quarter front view L-78185.1

(a) Model A.

Figure 2.- Photographs of model A and model B.

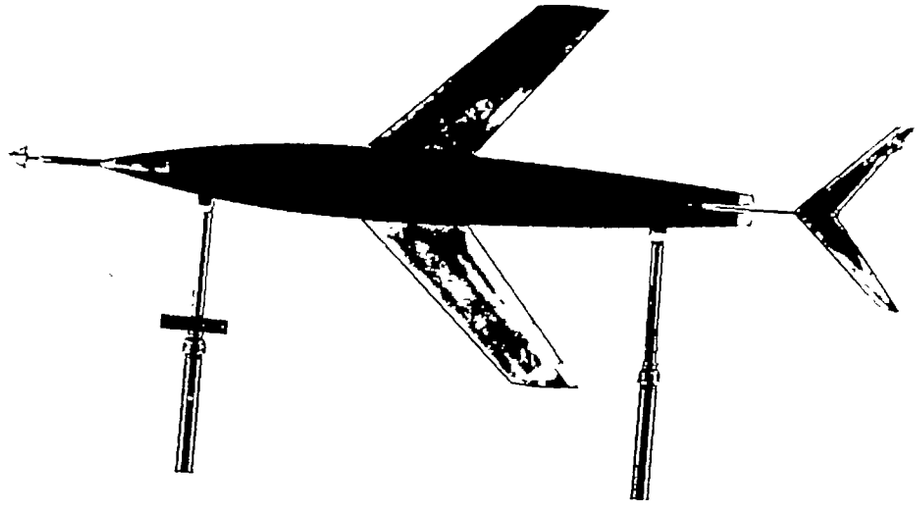

Top view L-76251.1

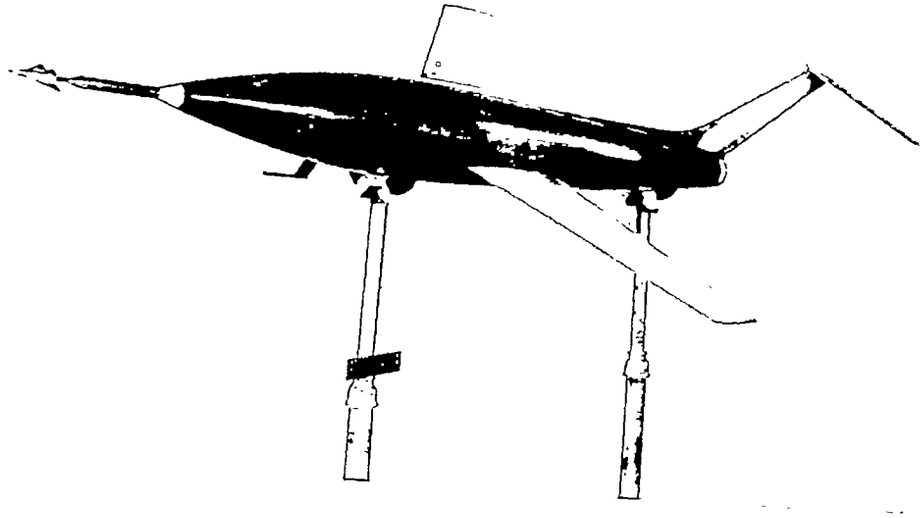

Three-quarter front view L-76250.1

(b) Model B.

Figure 2.- Concluded.

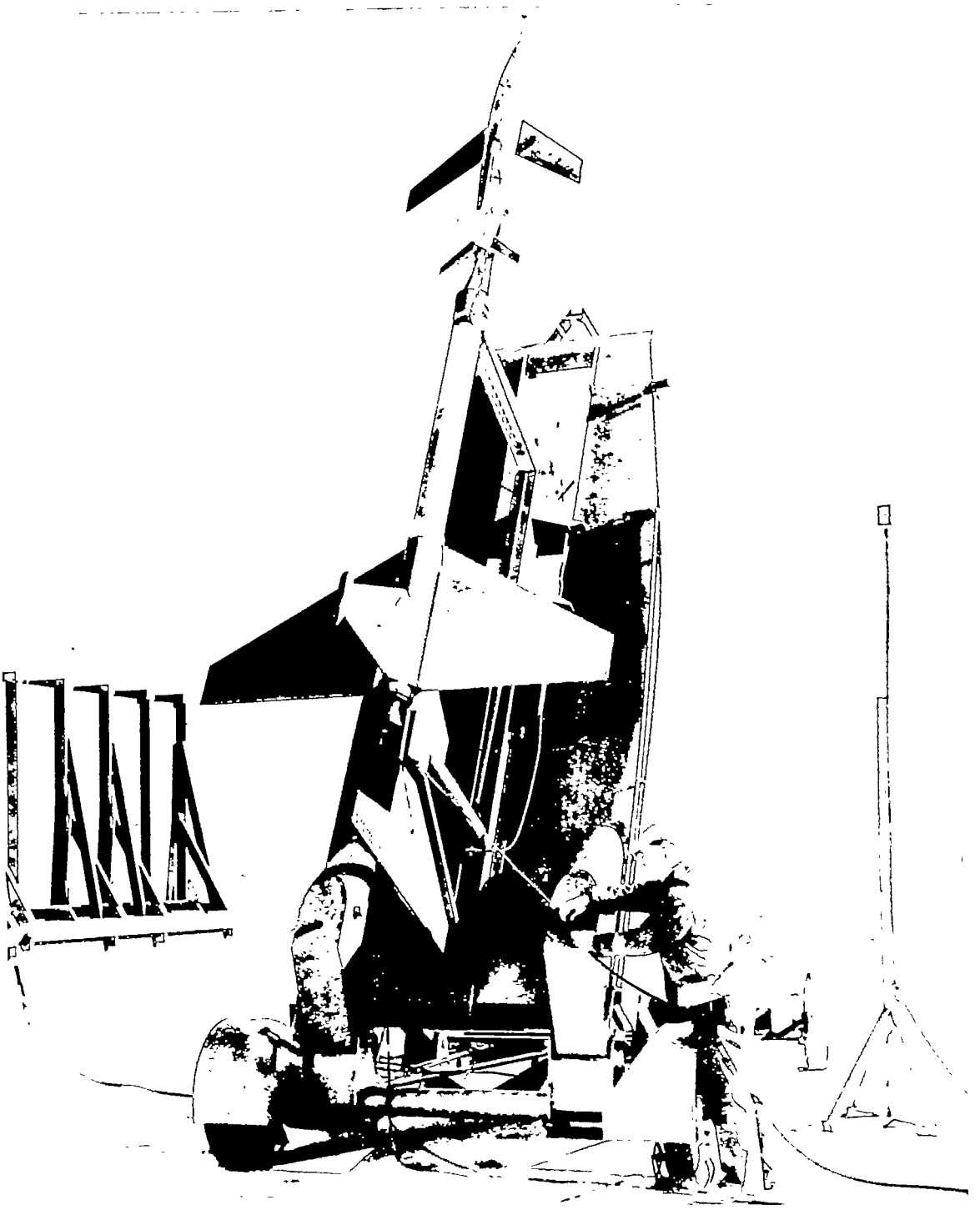

L-78395.1

Figure 3.- Model-booster combination on launching platform.

[redacted]

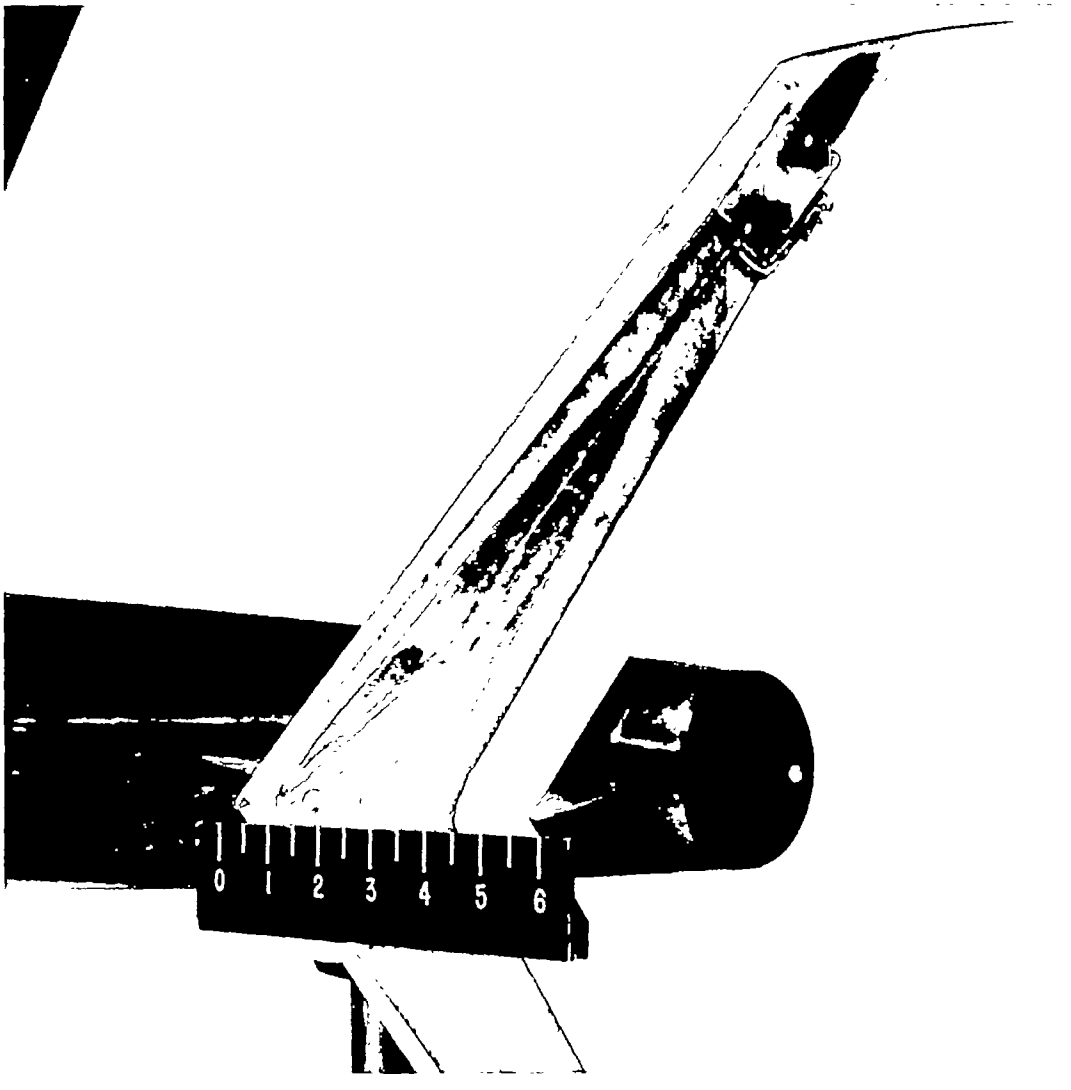

L-76253

Figure 4.- Typical installation of horizontal-tail vibrometer.

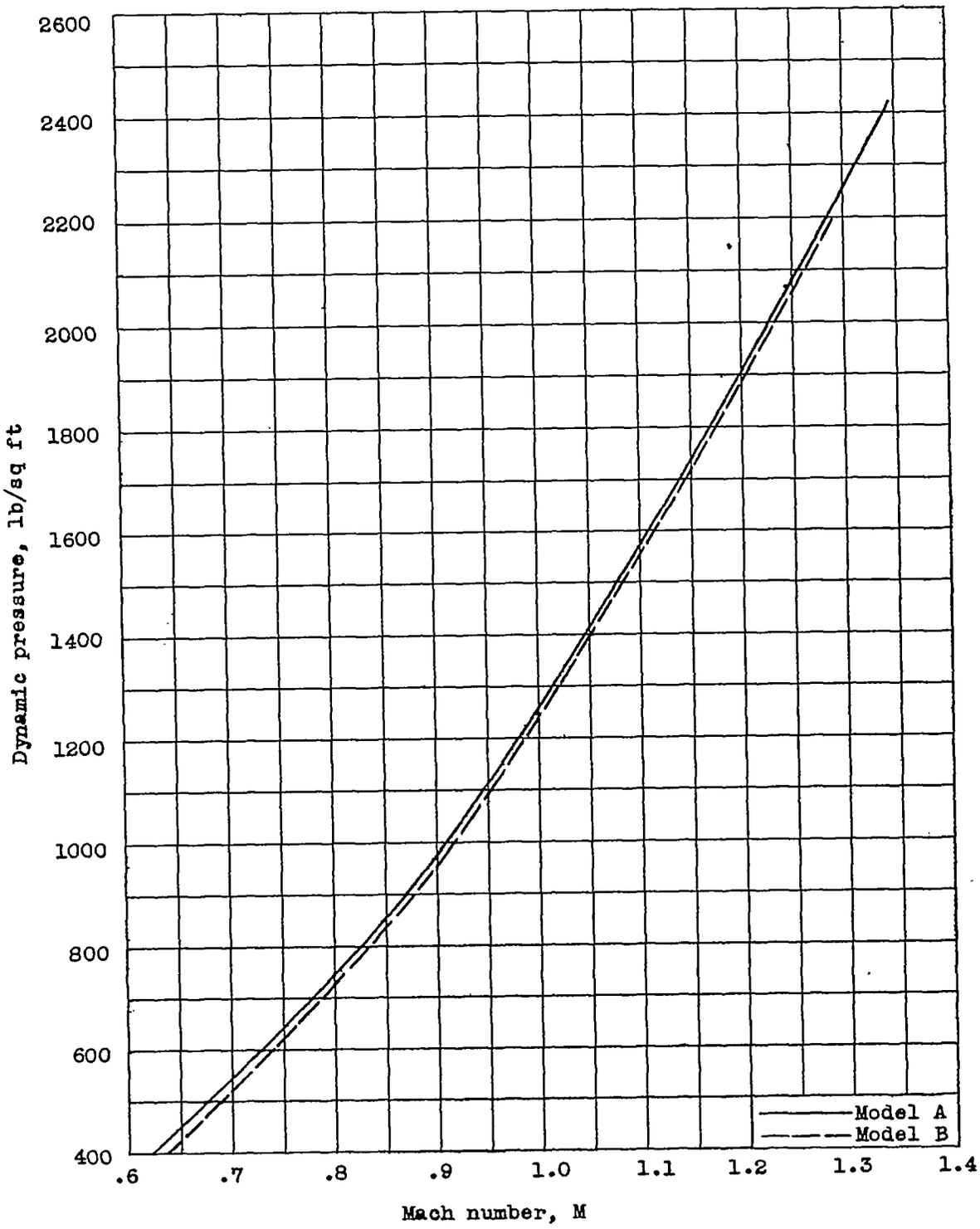

Figure 5.- Variation of dynamic pressure with Mach number.

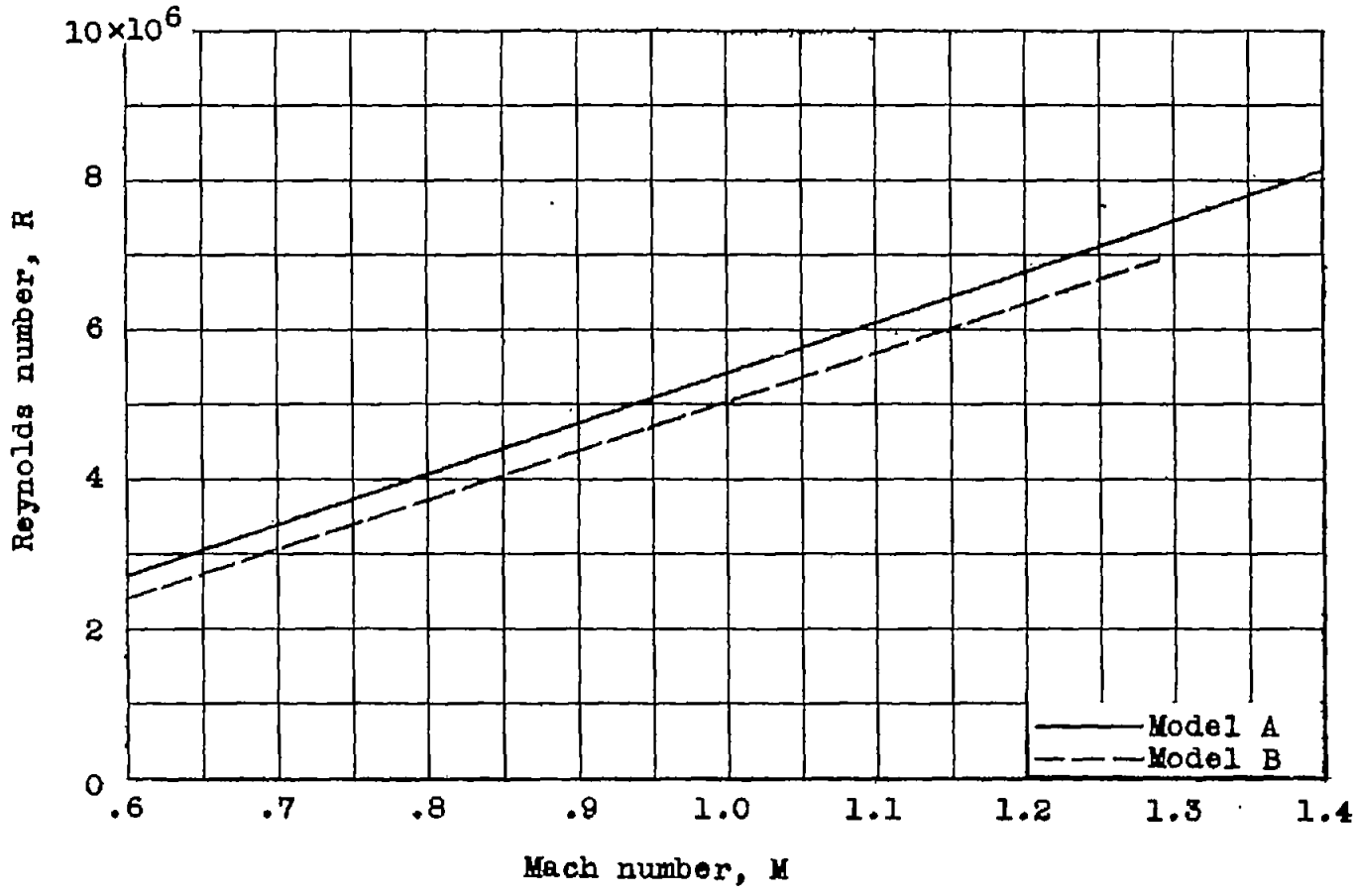

Figure 6.- Variation of Reynolds number with Mach number.

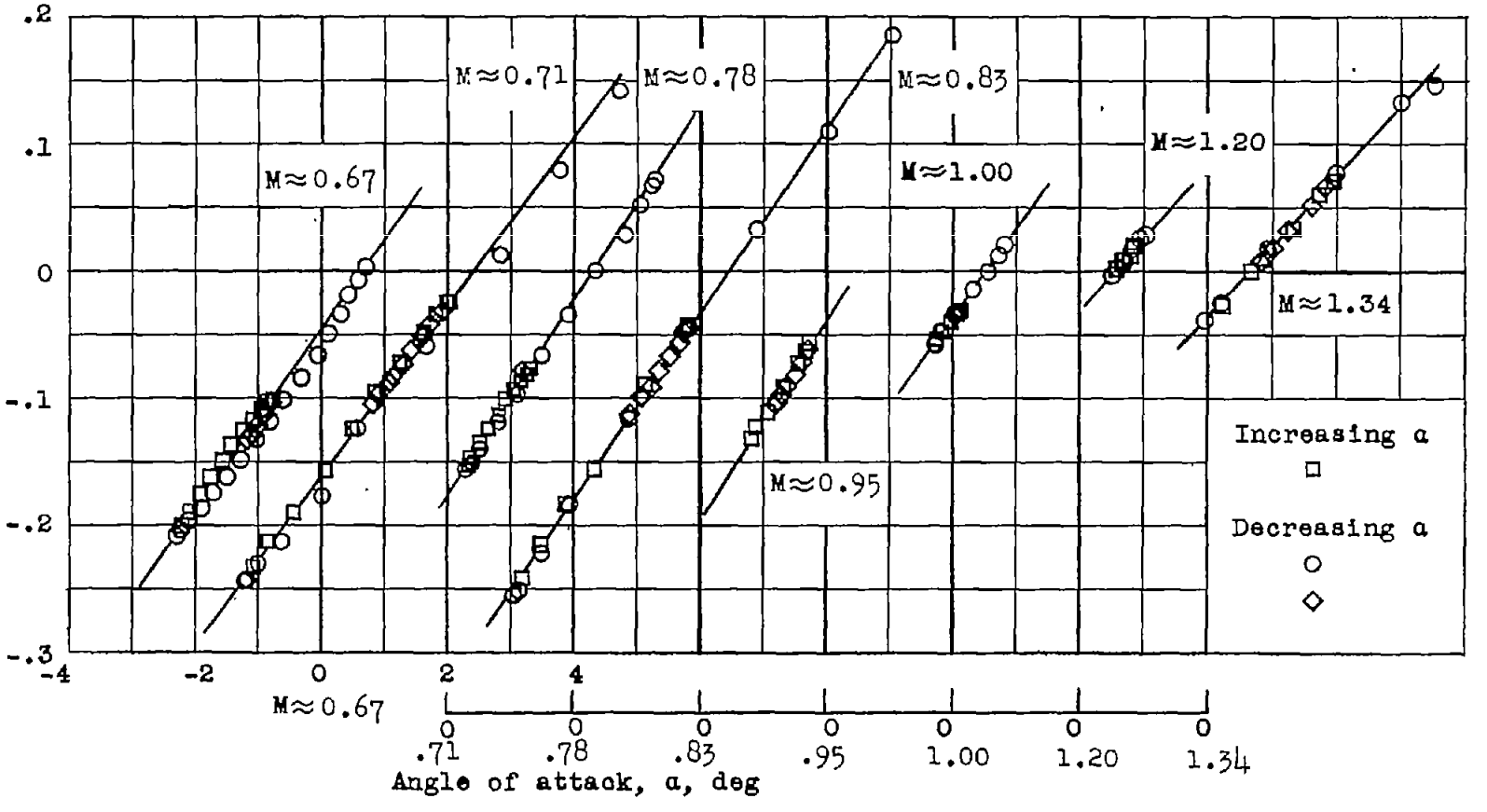

(a) Model A.

Figure 7.- Lift-curve data obtained from the short period oscillations.

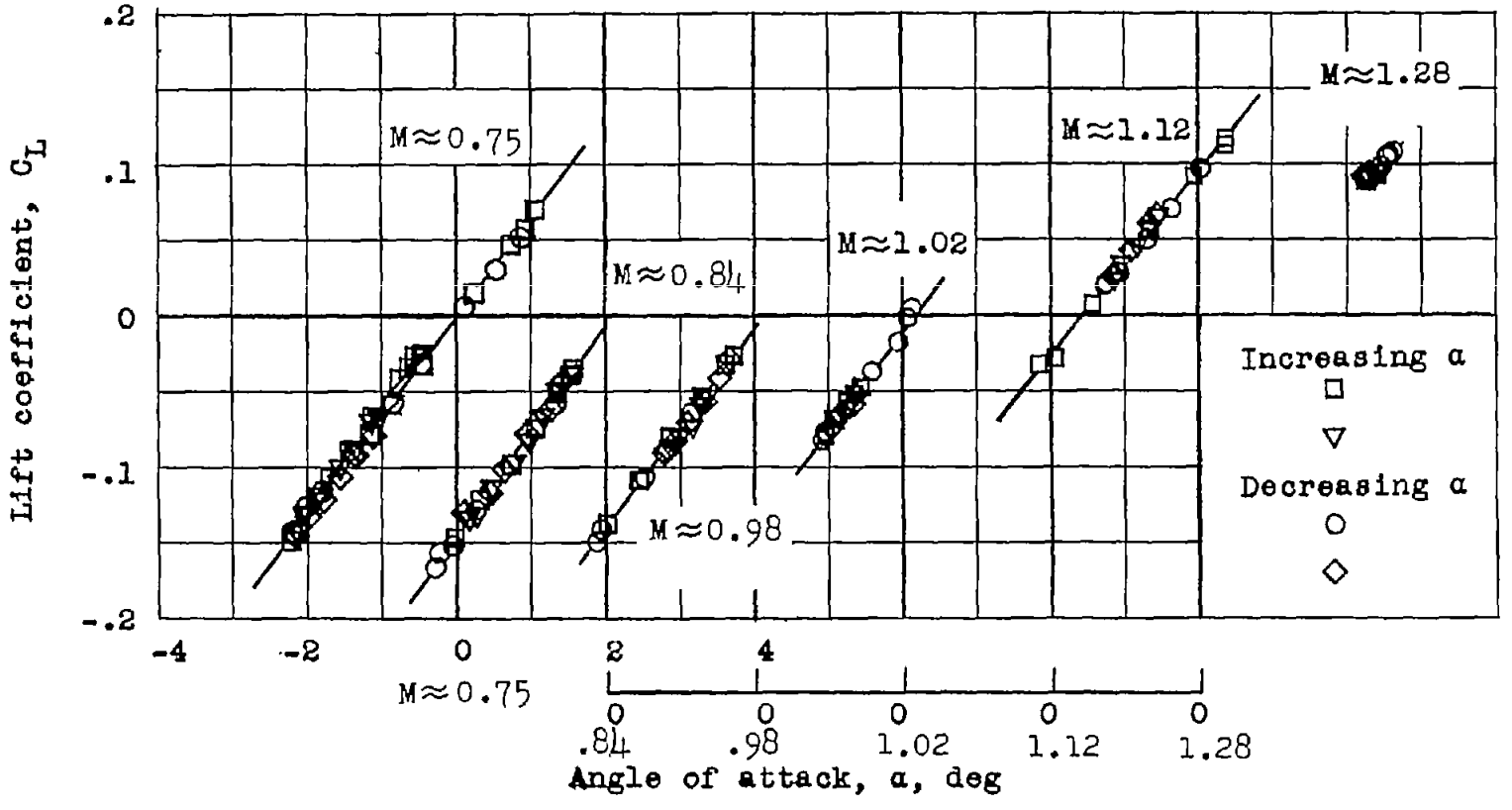

(b) Model B.

Figure 7.- Concluded.

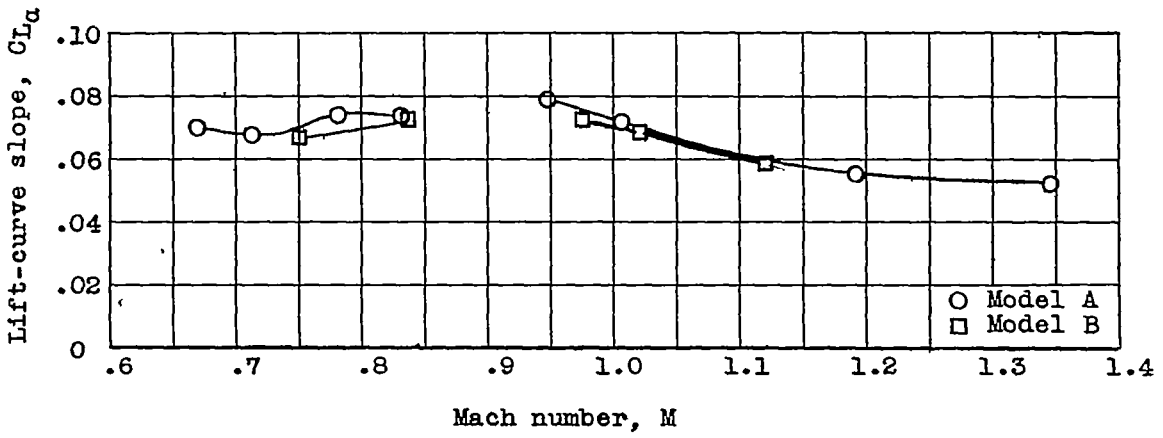

Figure 8.- Variation of the lift-curve slope with Mach number.

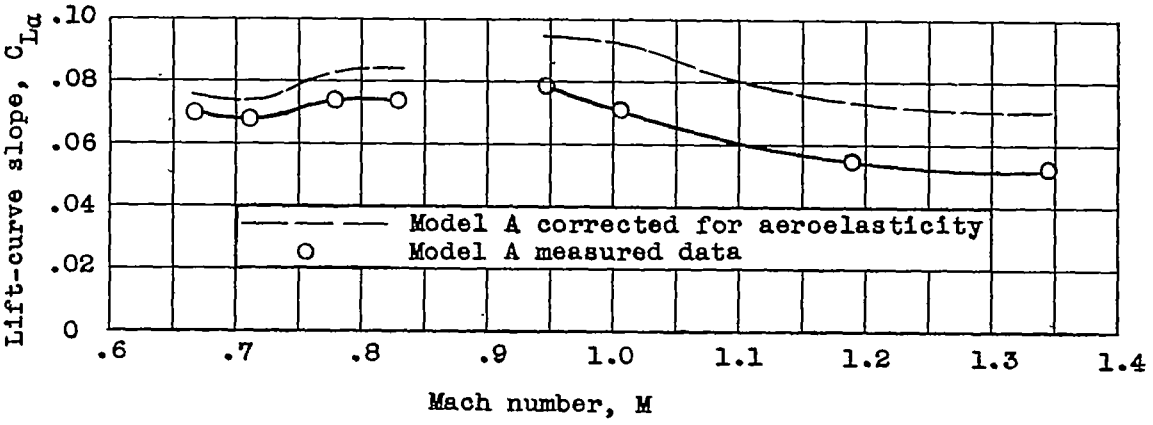

Figure 9.- Comparison of the lift-curve slope of model A with and without the effects of aeroelasticity considered.

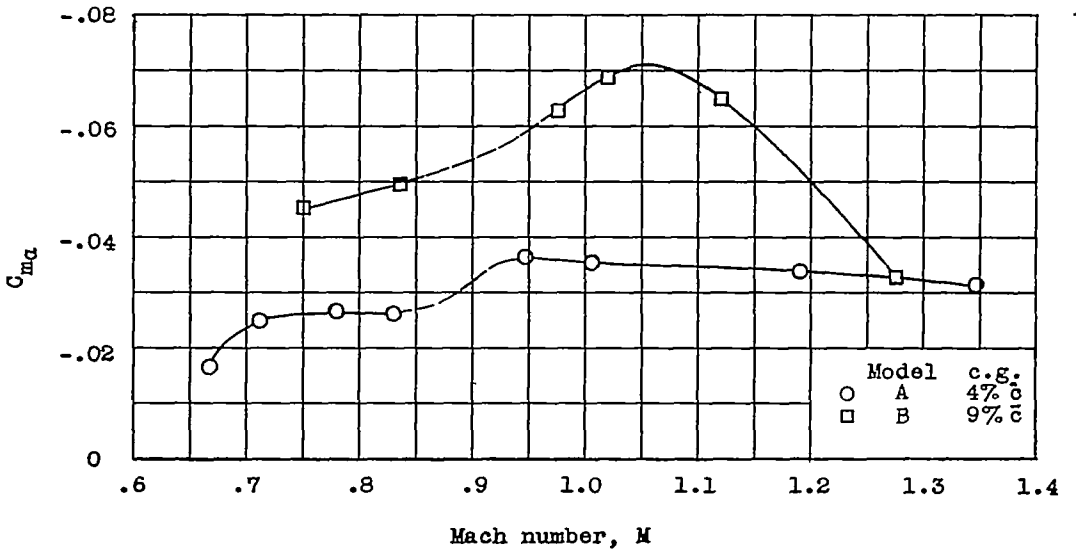

Figure 10.- Variation of the static stability parameter with Mach number.

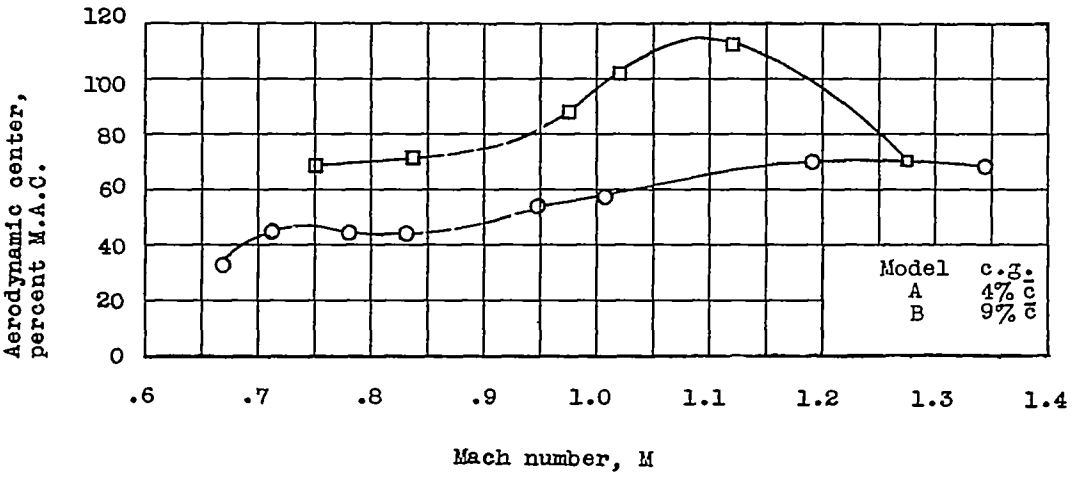

Figure 11.- Variation of the aerodynamic-center location with Mach number.

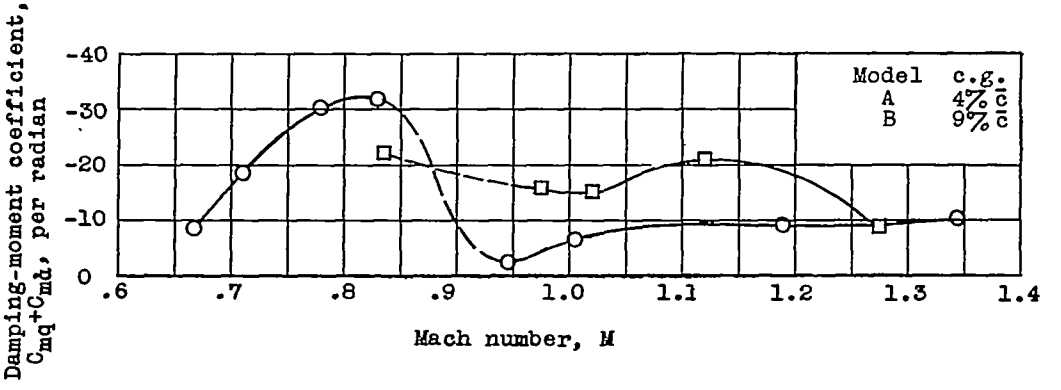

Figure 12.- Variation of damping-moment [redacted]ficient with Mach number.

[redacted]

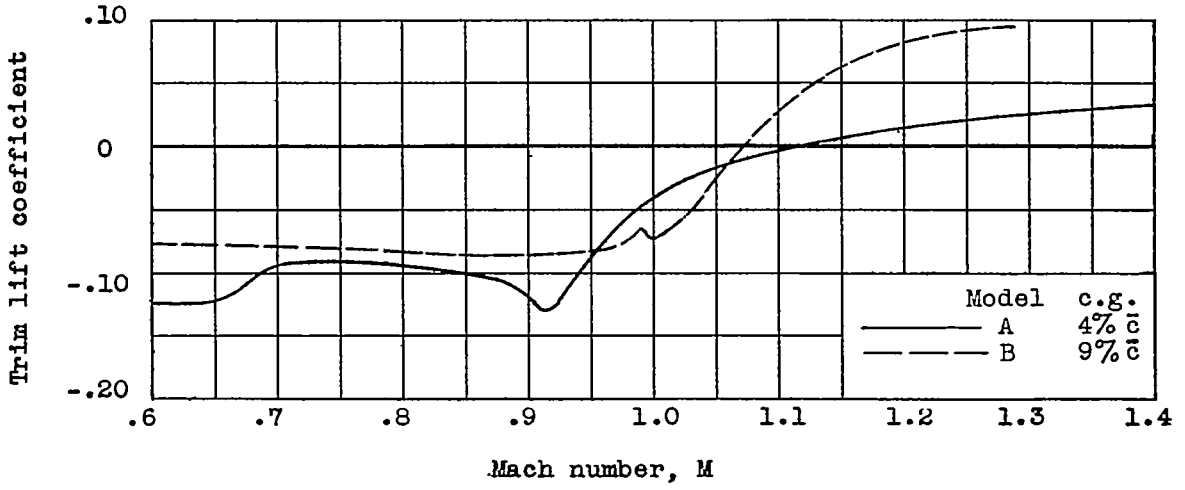

(a) Lift coefficient.

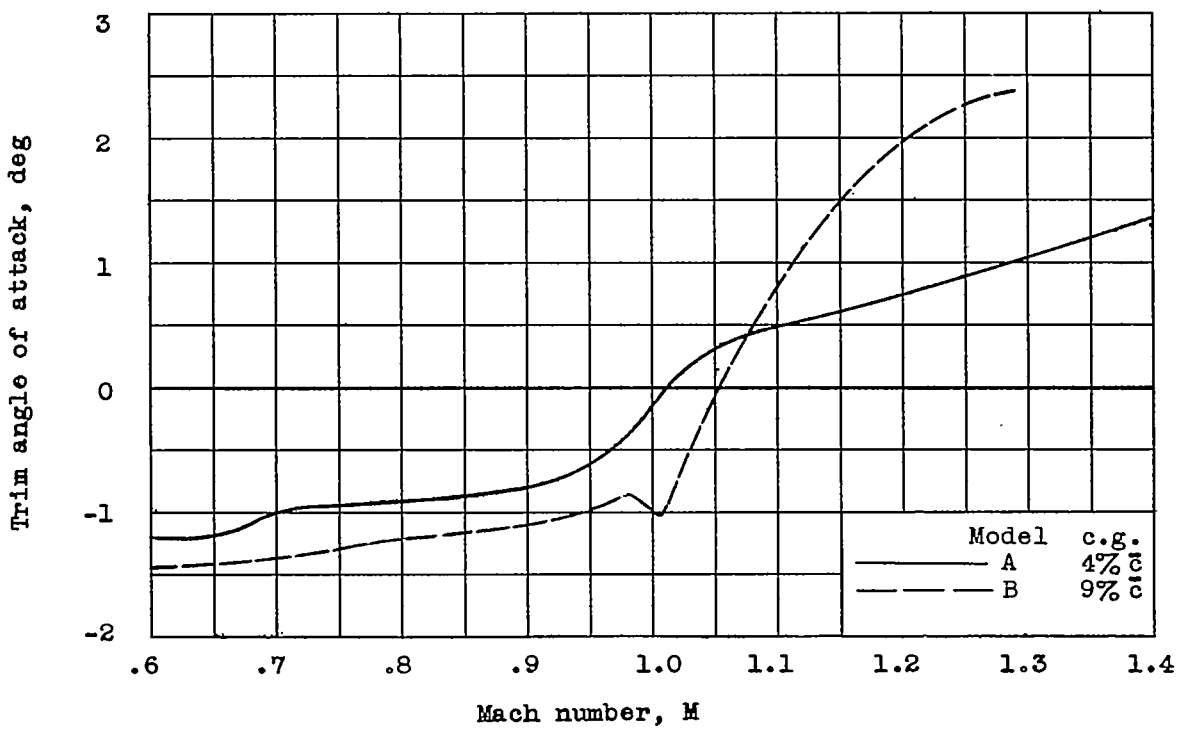

(b) Angle of attack.

Figure 13.- Longitudinal trim characteristics as a function of Mach number.

Basic frequencies

Model A	cps	Model B	cps
Wing 1st bending	53	Wing 1st bending	46
Horiz. tail 1st bending	78	Horiz. tail 1st bending	58
Vertical tail 1st bending	117	Vert. tail 1st bending	32
Wing 2nd bending	246	Wing 2nd bending	208
Wing torsion	355	Wing torsion	296
Horiz. tail 2nd bending	450	Horiz. tail 2nd bending	299

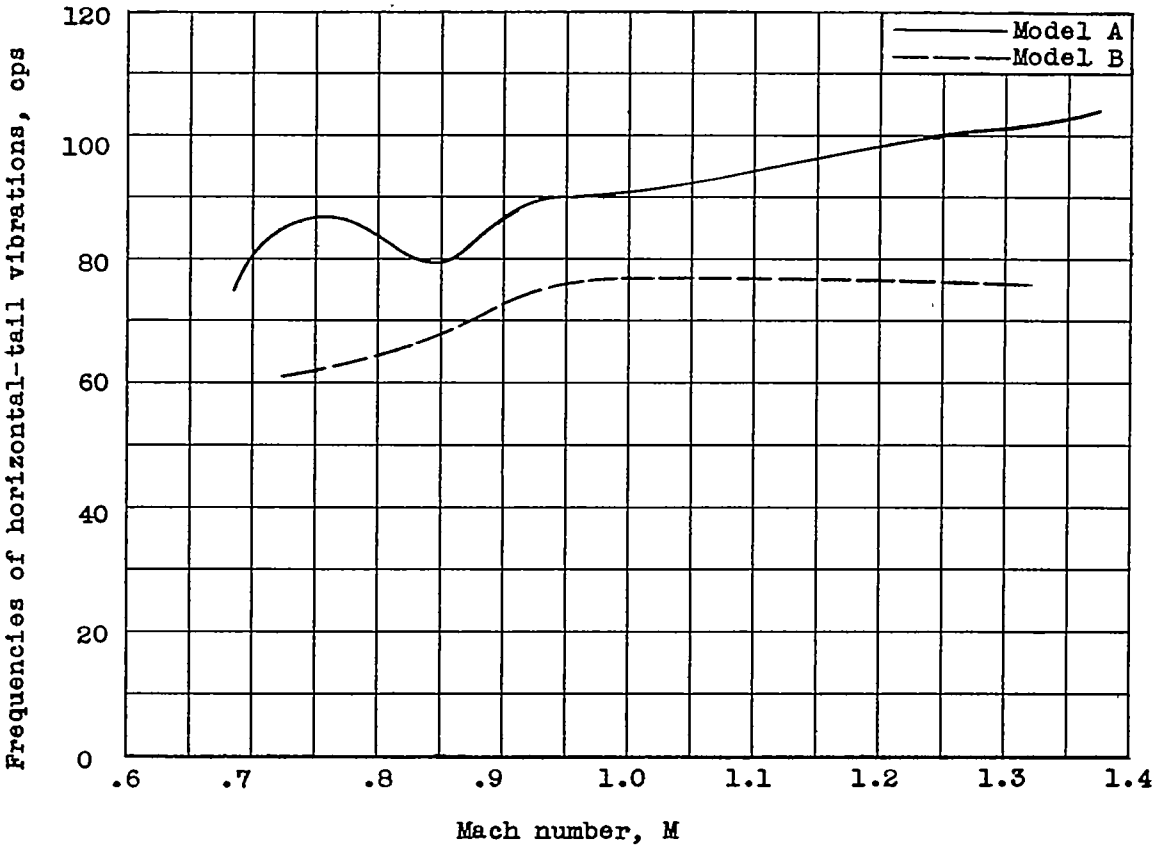

Figure 14.- Variation of horizontal tail vibrations with Mach number.

[redacted]

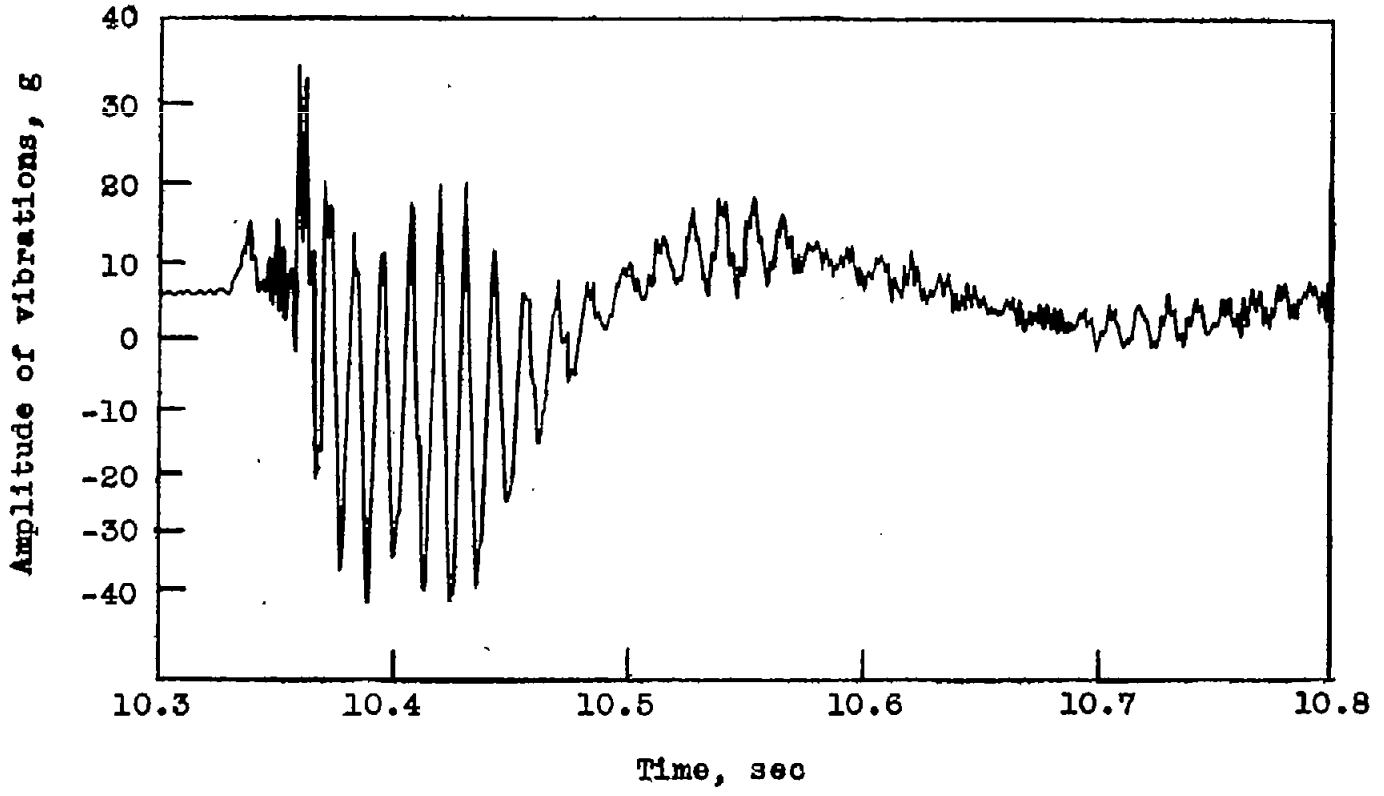

(a) Model A; M = 0.73 to 0.71.

Figure 15.- Variation of amplitude of vibrations of horizontal-tail vibrometer with time for model A and model B.

[redacted]

CONFIDENTIAL

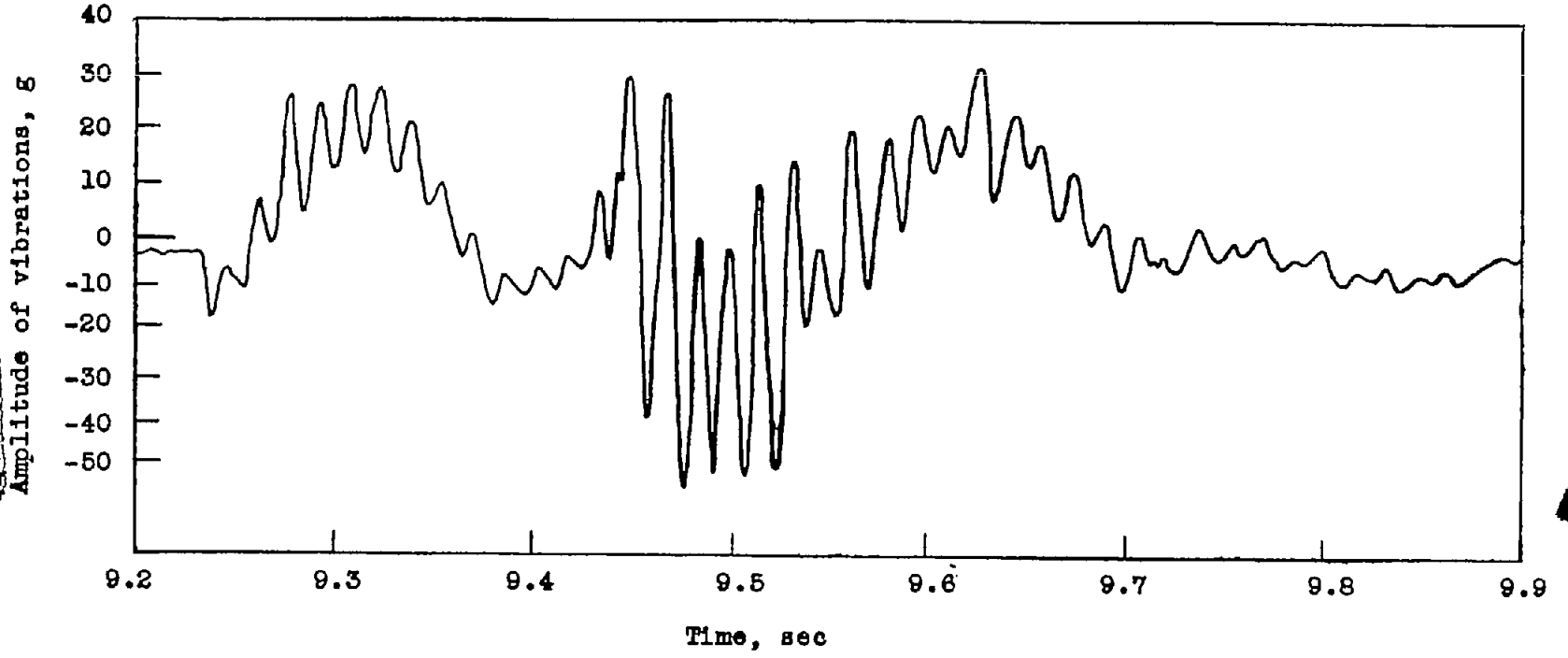

(b) Model B; M = 0.77 to 0.75.

Figure 15.- Concluded.

CONFIDENTIAL

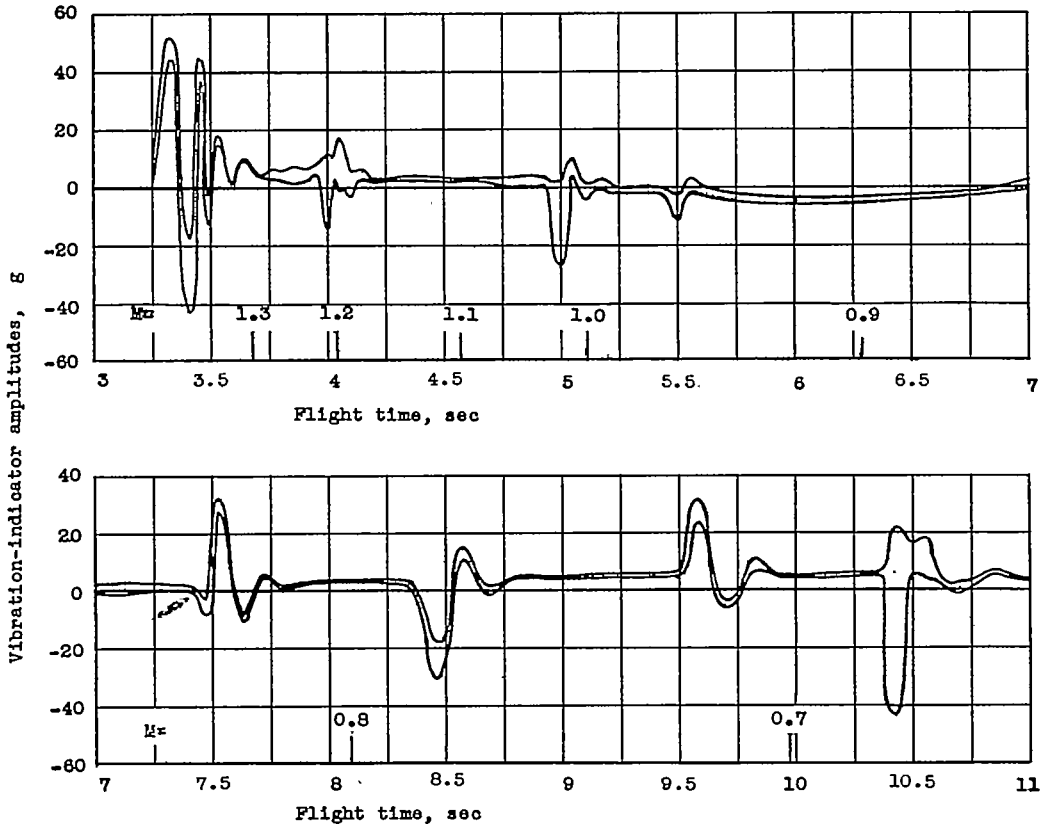

(a) Model A.

Figure 16.- Time-history of the amplitude envelopes indicated by the vibration indicators.

CONFIDENTIAL

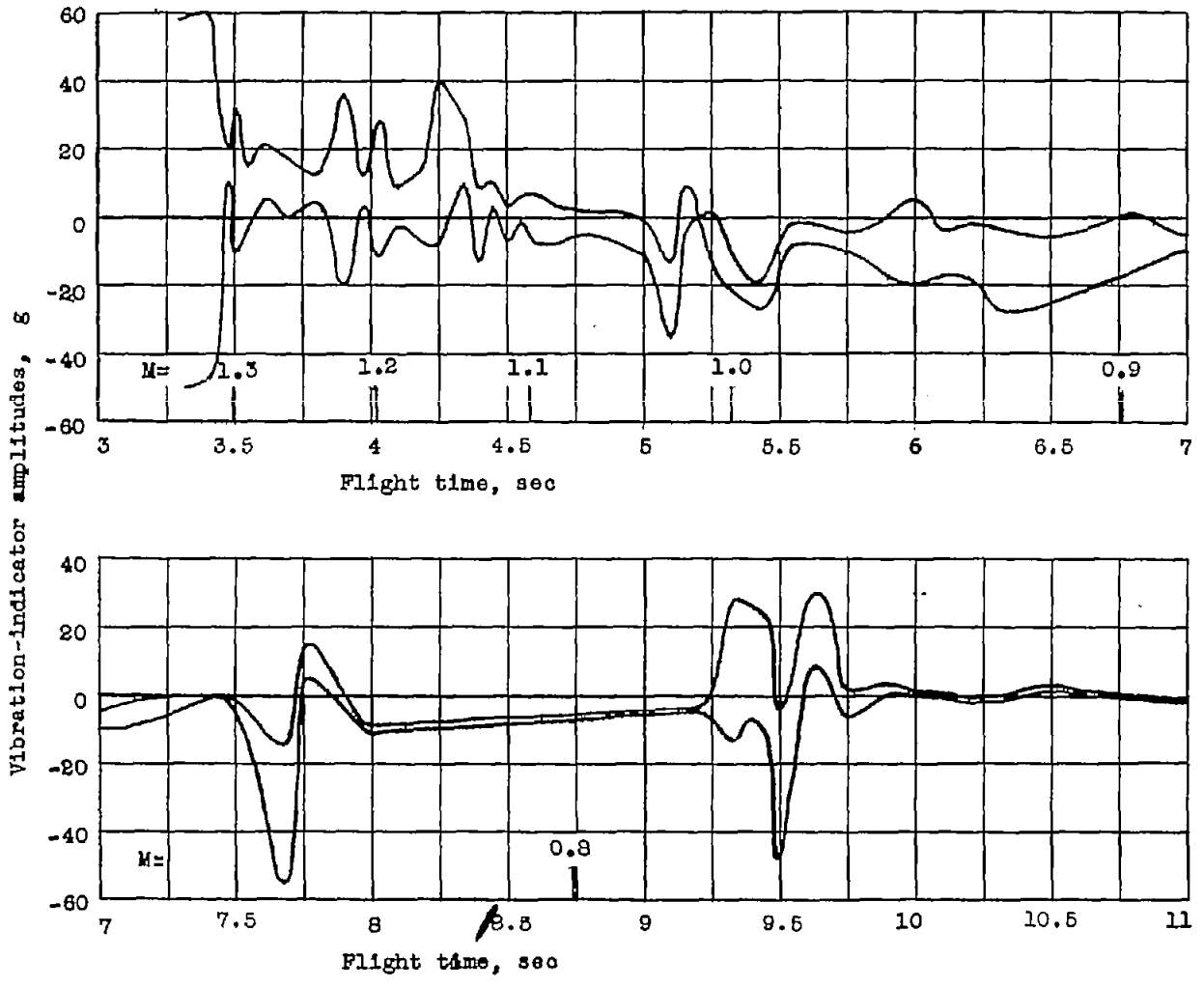

(b) Model B.

Figure 16.- Concluded.

CONFIDENTIAL

NACA-Langley - 12-9-53 - 325